Supporting Information

Reactive Suspension Electrolytes for Lithium Metal Batteries

Junyoung Lee[1#], Mun Sek Kim[2#], Yi Cui[1], Wenbo Zhang[1], Sanzeeda Baig Shuchi[2], Sarah E. Holmes[3], Jun Ho Lee[1], Chad Serrao[1], Sang Cheol Kim[4], John Holoubek[1], Philaphon Sayavong[3], Angela Cai[1], Il Rok Choi[1], Yi Cui[1,5,6*]

[1]Department of Materials Science and Engineering, Stanford University, Stanford, California 94305, United States.

[2]Department of Chemical Engineering, Stanford University, Stanford, California 94305, United States.

[3]Department of Chemistry, Stanford University, California 94305, United States.

[4]Department of Physics, Stanford University, California 94305, United States.

[5]Department of Energy Science and Engineering, Stanford University, California 94305, United States.

[6]Stanford Institute for Materials and Energy Sciences, SLAC National Accelerator Laboratory, Menlo Park, California 94025, United States.

[#]J.L. and M.S.K. contributed equally to this work.

*email: yicui@stanford.edu

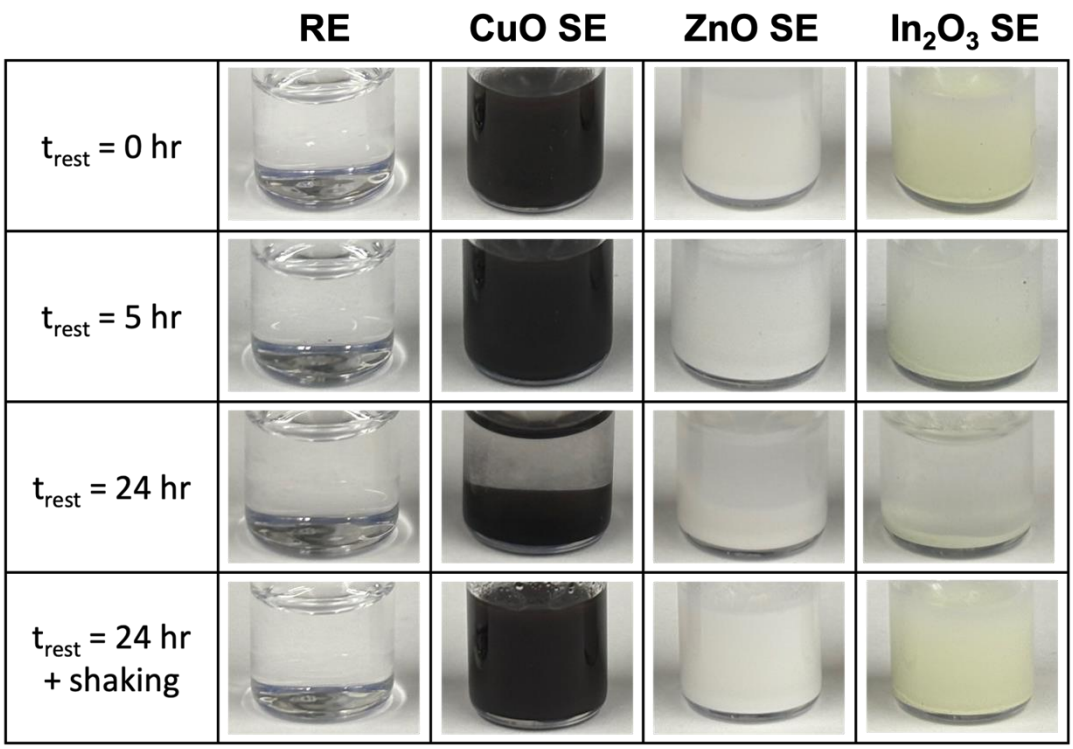

Figure S1. Time-lapse images of RE, CuO RSE, ZnO RSE, and In_2O_3 RSE. Suspended nanoparticles settle over time due to gravity, but they can be readily redispersed by gently shaking the electrolyte several times.

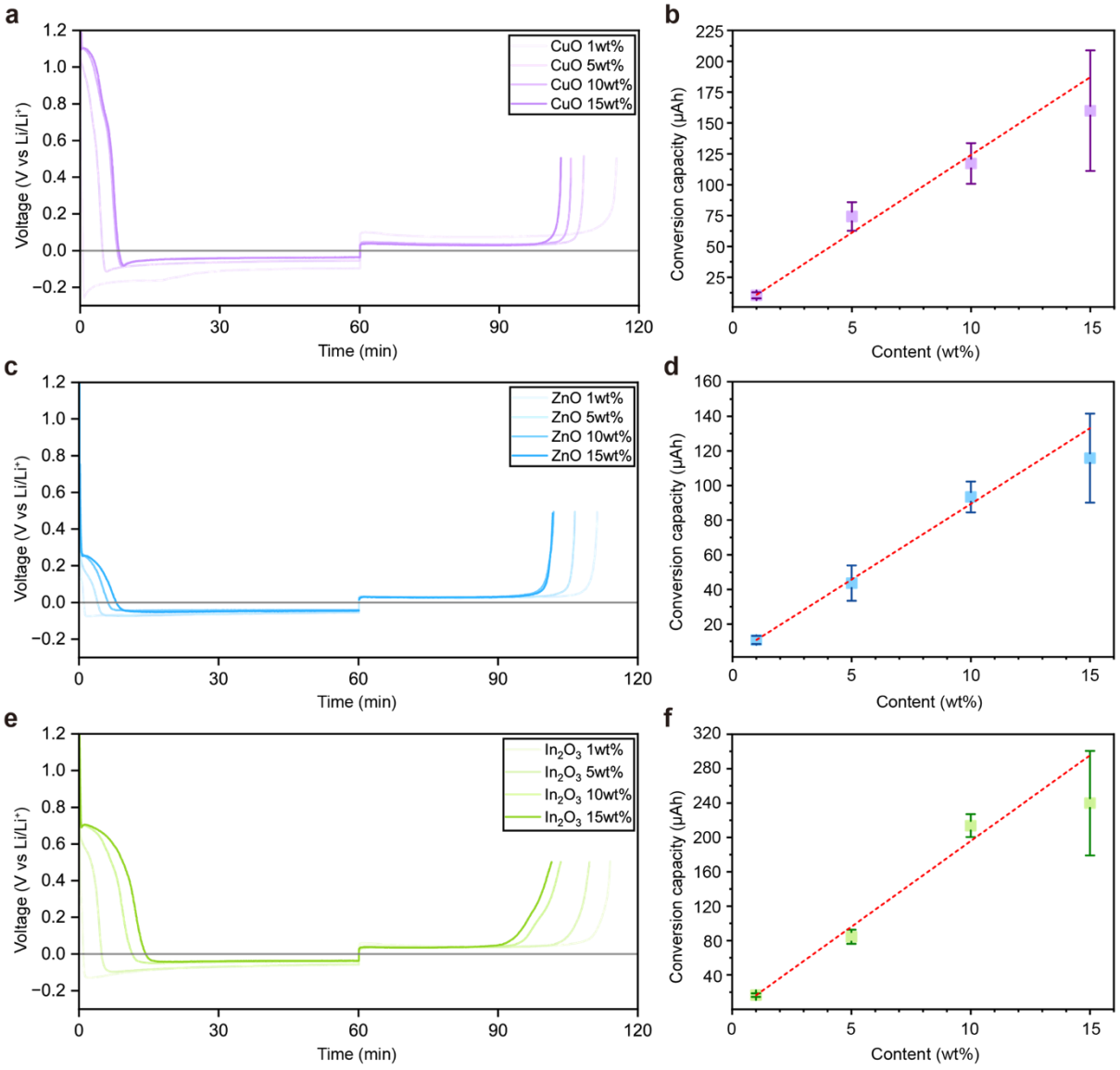

Figure S2. Galvanostatic voltage profiles of RSEs during Li plating and stripping depending on a suspension content. Li|Cu cell with each RSE was discharged and charged at 1 mA cm^{-2}, 1mAh cm^{-2}. The definition of consumption capacity is explained in the Experimental section. a) Voltage profiles of CuO RSEs (1-15 wt%) and b) consumption capacity versus content of CuO NPs. c) Voltage profiles of ZnO RSEs (1-15 wt%) and d) consumption capacity versus content of ZnO NPs. e) Voltage profiles of In_2O_3 RSEs (1-15 wt%) and f) consumption capacity versus content of In_2O_3 NPs.

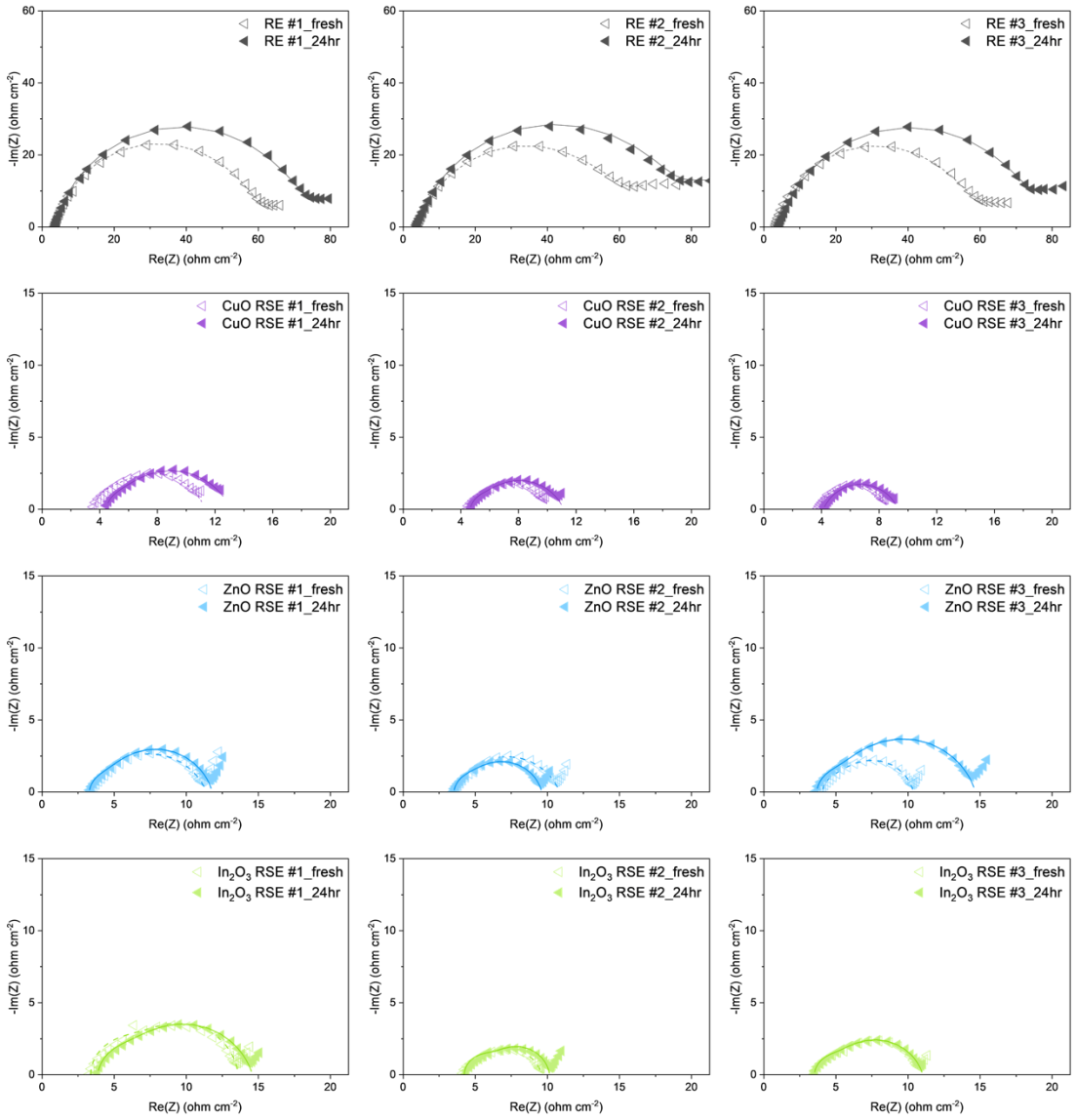

Figure S3. Nyquist plots from Li|Cu cell with RE and RSEs after plating of 1 mAh cm^{-2}. Plots were obtained from three replicates of (a) RE, (b) CuO RSE, (c) ZnO RSE, and (d) In_2O_3 RSE respectively. EIS measurements were performed two times for each cell; immediately after plating (denoted as "fresh", open symbol for raw data and dashed line for fitting) and after 24 h of resting (denoted as "24hr", occupied symbol for raw data and solid line for fitting).

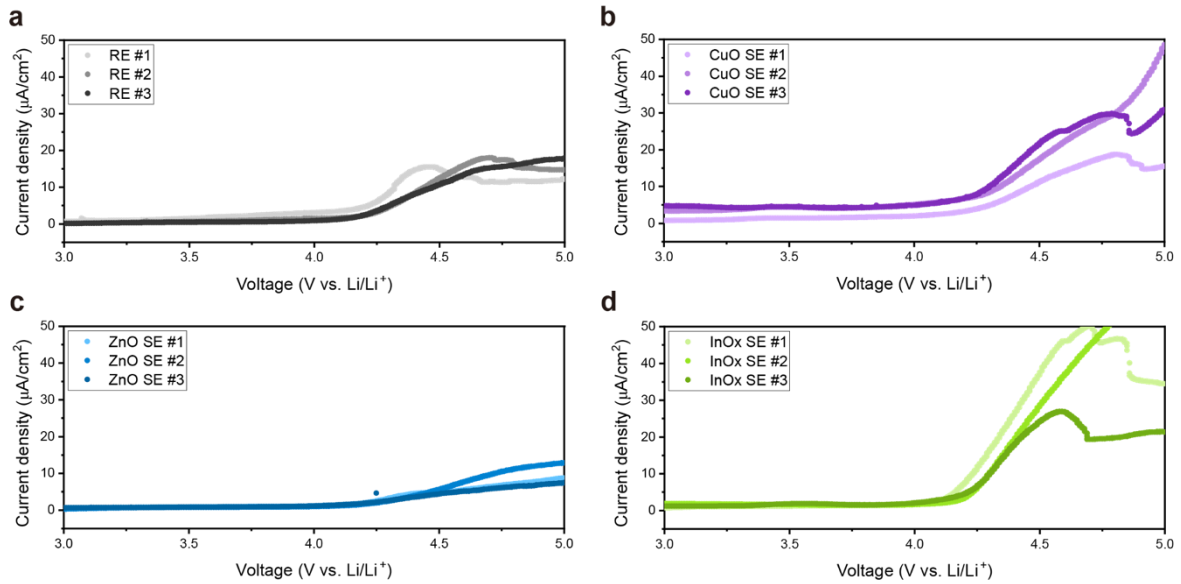

Figure S4. Linear sweep voltammetry (LSV; from open circuit voltage (OCV) to 5.0 V vs. Li/Li^+) results with a) RE, b) CuO RSE, c) ZnO RSE, and d) In_2O_3 RSE using Li|Al cell. Each cell was scanned at 1 mV s^{-1}.

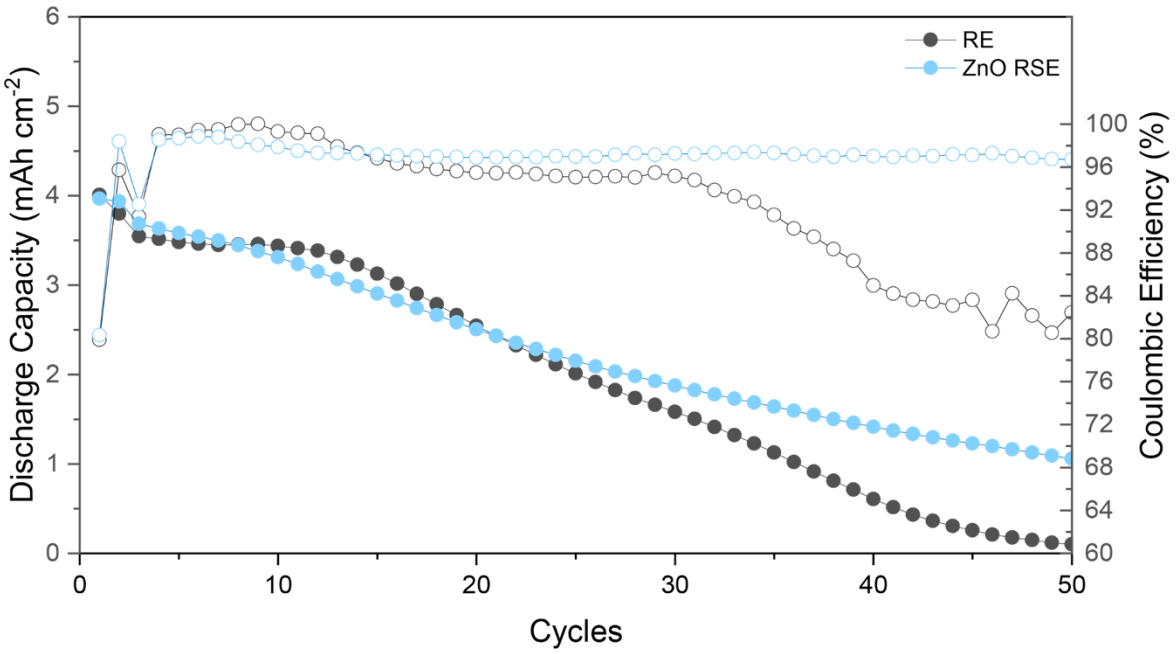

Figure S5. Representative Cu|NMC811 full cell cycling (between 3.0 V and 4.3 V vs. Li/Li^+) profiles of discharge capacity (filled symbols) and Coulombic efficiency (open symbols) with RE and three different RSEs. Cells were initially charged at 0.2 C and discharged at 0.5 C two times as activation cycles, followed by cycling at 0.5 C charging (0.5C) and 1.0C discharging (1.0D).

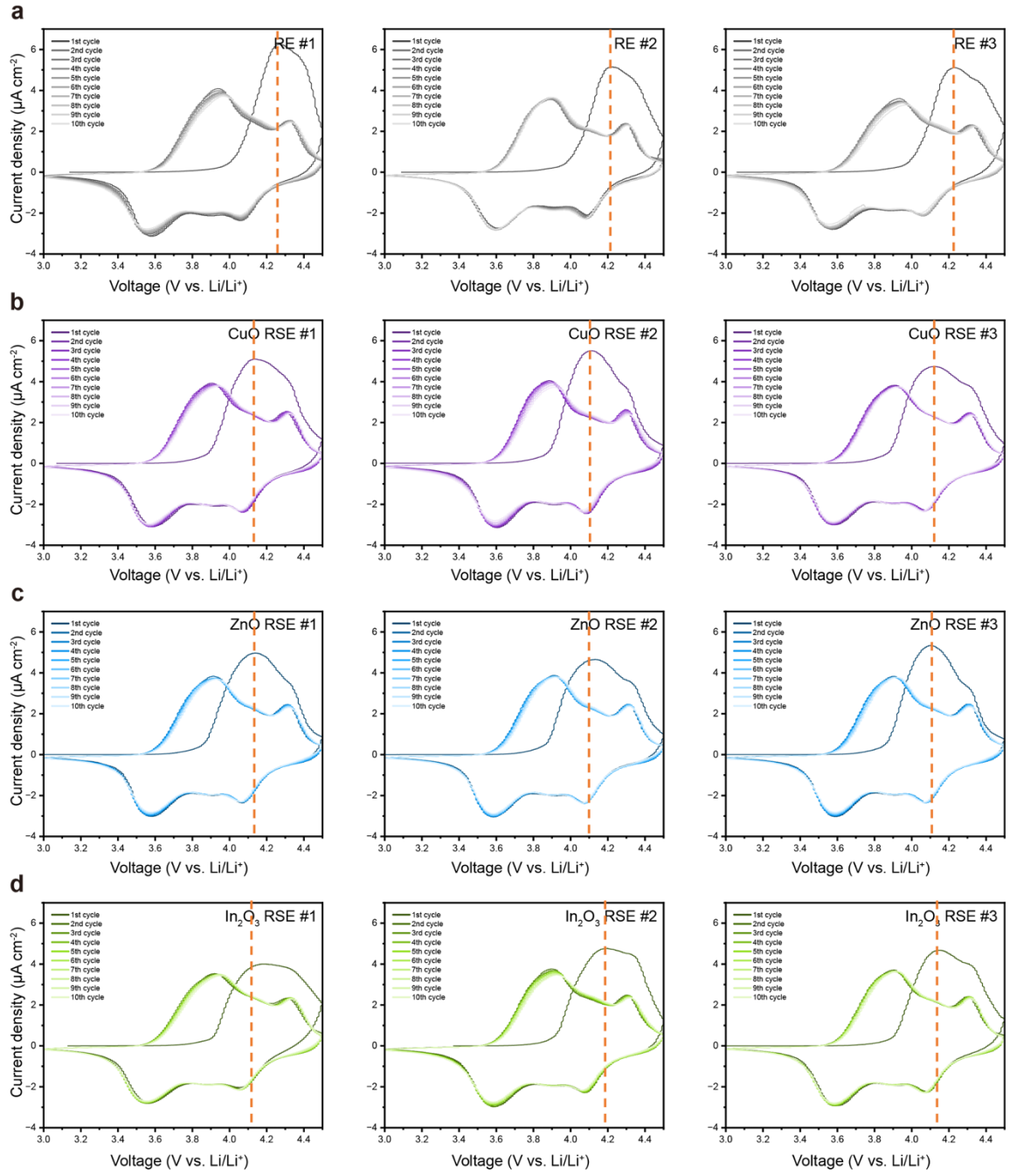

Figure S6. First 10 cycle cyclic voltammetry (CV; from 3.0 to 4.5 V vs. Li/Li^+) results with (a) RE, (b) CuO RSE, (c) ZnO RSE, and (d) In_2O_3 RSE using $Li|Li_1Ni_{0.8}Mo_{0.1}Co_{0.1}O_2$ (NMC811) cells. Each full cell was scanned at 0.1 mV s^{-1}. The dashed orange line indicates the first charging redox potential.

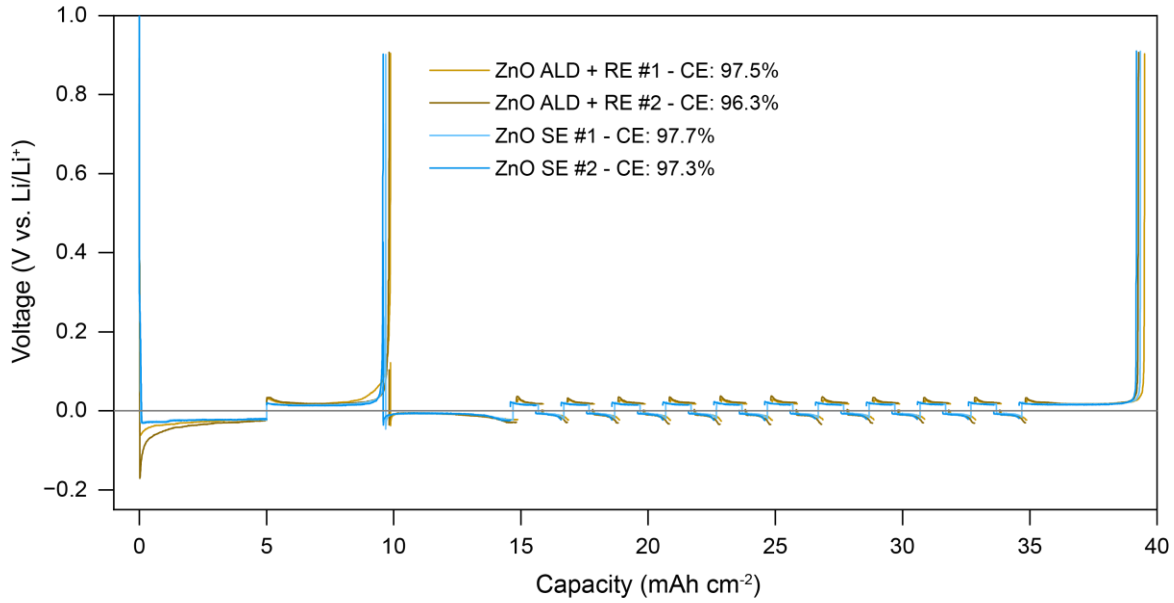

Figure S7. Comparison between ALD-coated ZnO and ZnO RSE. Representative half cell voltage profiles of CE measurement scanned at a current density of 0.5 mA cm^{-2}. Yellowish lines indicate the data from Li|ZnO-coated Cu cell with RE while bluish lines represent the data from Li|Cu cell with ZnO RSE. ZnO RSE exhibited smaller nuclear overpotential than ALD-coated ZnO sample during the first lithiation.

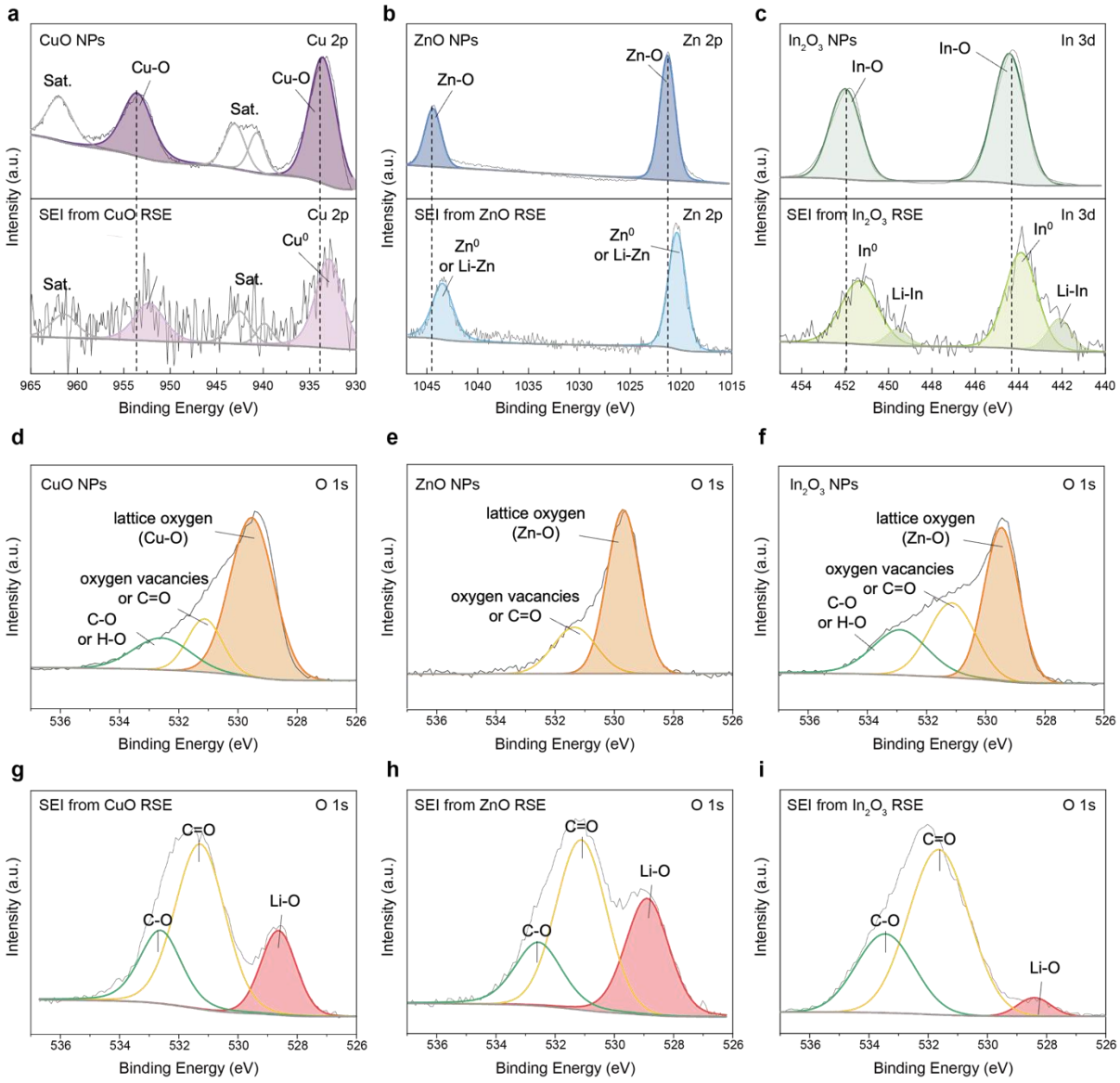

Figure S8. XPS analyses on bare MO_x nanoparticles and MO_x RSE-derived SEIs. a-c) High-resolution XPS spectra of M species from bare MO_x nanoparticles and initially formed SEIs with RSE counterparts. From left to right, (a) Cu 2p spectra of CuO NPs (top) and SEI from CuO RSE (bottom), (b) Zn 2p spectra of ZnO NPs (top) and SEI from ZnO RSE (bottom), and (c) In 3d spectra of In_2O_3 NPs (top) and SEI from In_2O_3 RSE (bottom). d-f) High resolution XPS O 1s spectra from bare MO_x nanoparticles. For left to right, (d) CuO NPs, (e) ZnO NPs, and (f) In_2O_3 NPs. g-i) High resolution XPS O 1s spectra from initially formed SEIs with RSEs. For left to right, (d) SEI from CuO RSE, (e) SEI from ZnO RSE, and (f) SEI from In_2O_3 RSE.

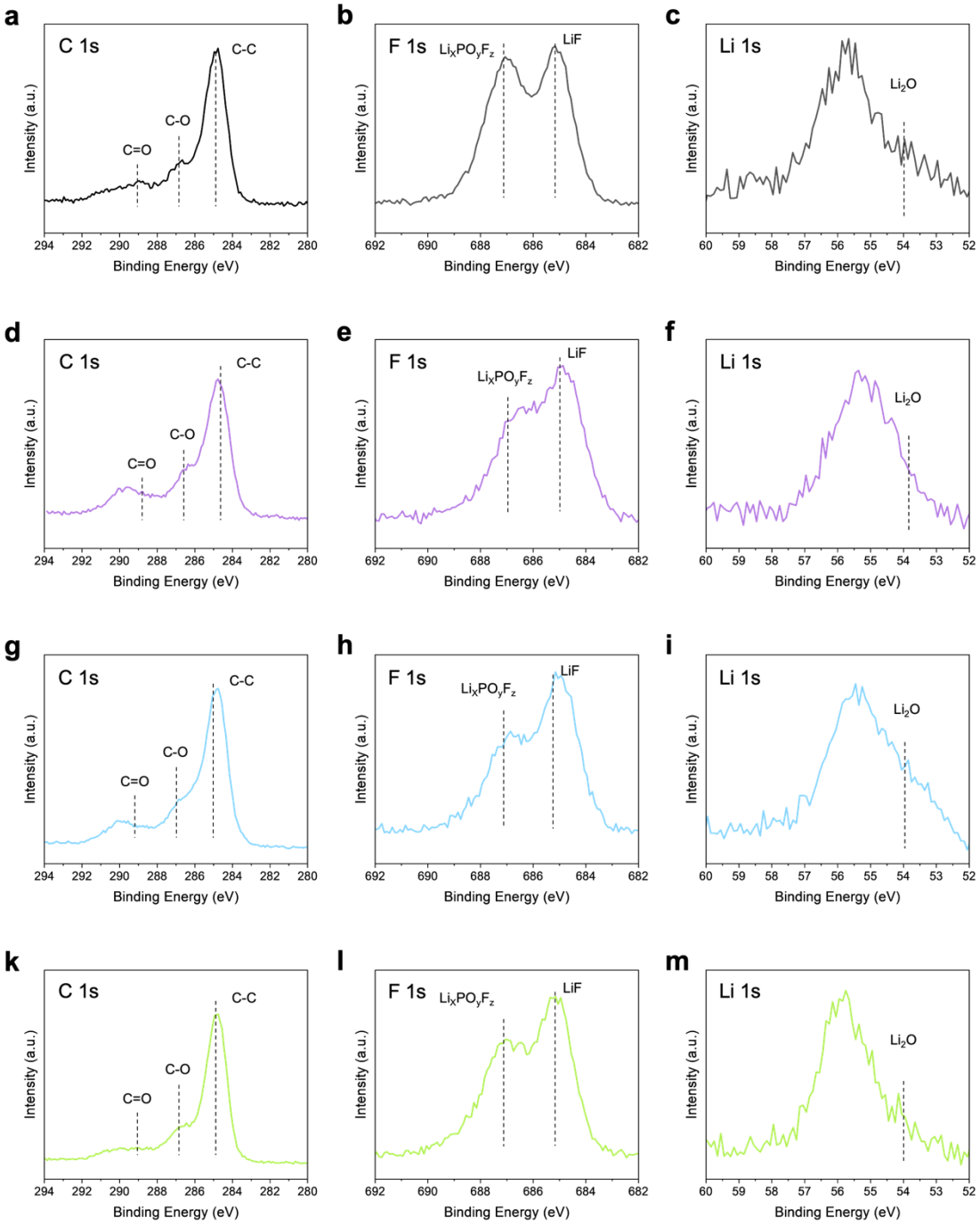

Figure S9. High resolution XPS spectra from initially formed SEIs across electrolytes. For each row, C 1s, F 1s, and Li 1s spectra are displayed from left to right. a-c) XPS data of RE-derived SEI, d-f) XPS data from CuO RSE-derived SEI, g-i) XPS data from ZnO RSE-derived SEI, and k-m) XPS data from In_2O_3 RSE-derived SEI.

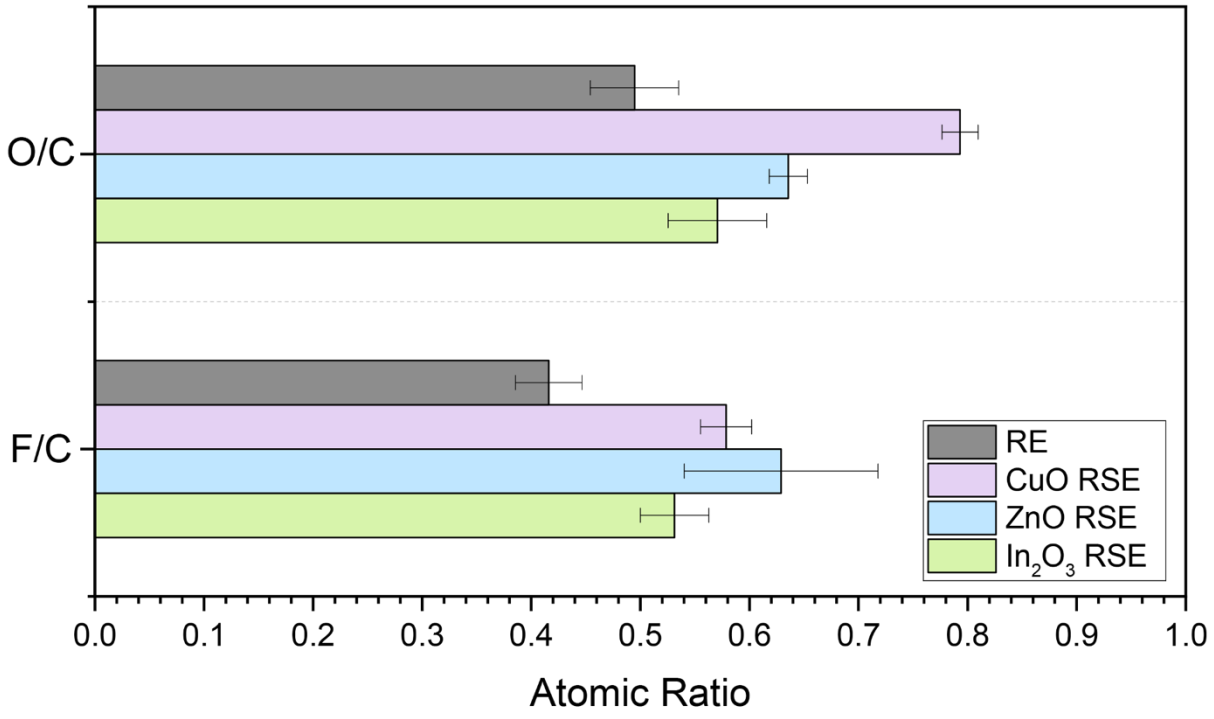

87

88 **Figure S10**. Elemental F/C and O/C ratios in SEIs of RE, CuO RSE, ZnO RSE, and In_2O_3

89 RSE, as determined from XPS scans.

90

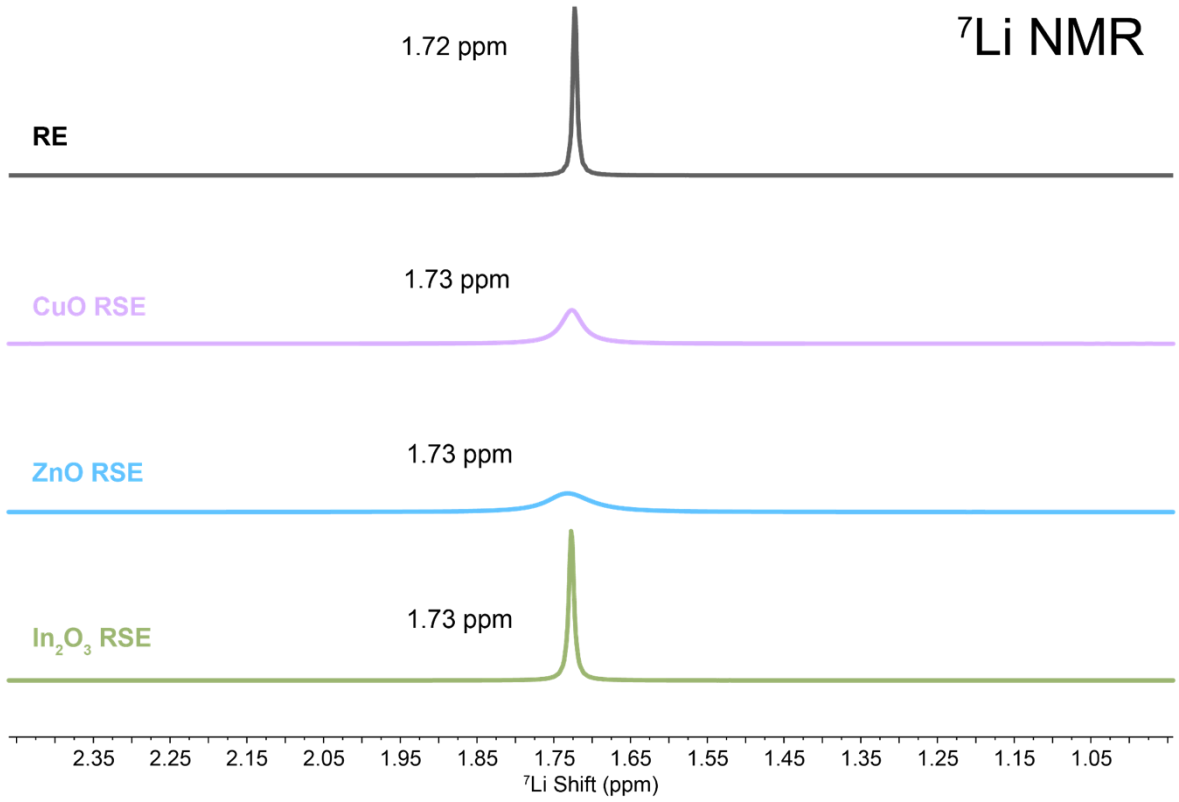

Figure S11. The ^{7}Li NMR spectra of RE, CuO RSE, ZnO RSE, and In_2O_3 RSE.

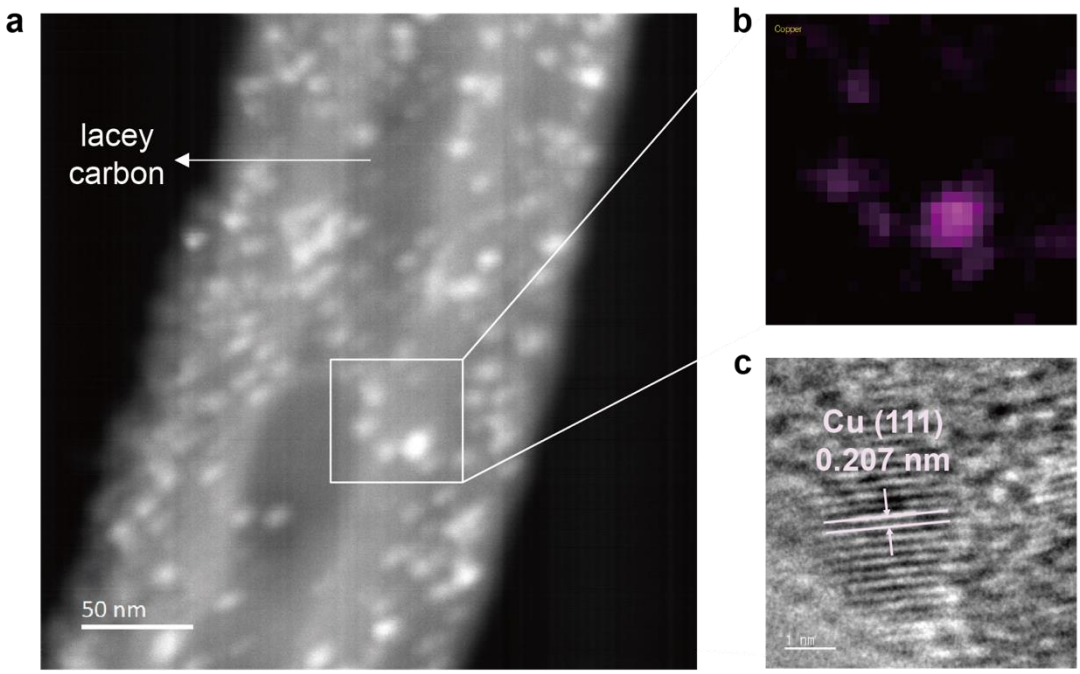

Figure S12. Cu nanoparticles generated from CuO RSE observed by Cryo-STEM and Cryo-TEM. a) Cryo-STEM ADF image of Cu nanoparticles on lacey carbon grid. b) Cryo-STEM EELS elemental mappings of Cu (purple). EELS spectra were acquired from the marked region in (a). c) High-resolution TEM image of an individual Cu nanoparticle with a fringe spacing of approximately 0.207 nm that corresponds to the (111) facet.

Experimental Section

Materials

All electrolytes and nanopowders were stored and handled inside Ar-filled glovebox with the designated O_2 level (< 0.2 ppm) and H_2O level (< 0.01 ppm). The reference electrolyte (RE) was made with 1M $LiPF_6$ in EC:DEC (1:1 v/v); LP40 (Sigma-Aldrich) with 10 vol % FEC (Gotion). For reactive suspension electrolyte, zinc oxide (ZnO) nanopowder (D < 100 nm, Sigma-Aldrich), indium(III) oxide (In_2O_3) nanopowder (D < 100 nm, Sigma-Aldrich), and copper(II) oxide (CuO) nanopowder (D < 50 nm, Sigma-Aldrich) were purchased and used without further purification. For cell fabrication, copper foil (Pred Materials), polyethylene separator (T = 11 µm, W-scope), high purity Li foil (T = 500 µm, Alfa Aesar), and ~4 mAh cm^{-2} NMC811 cathode (Targray) were used. Zinc oxide ALD was performed using Arradiance GEMStar^{TM} 6 Benchtop ALD system at 120 °C and film thickness was determined using a Si reference substrate using J.A. Woollam M2000 Variable Angle Spectroscopic Ellipsometer at 70° incident angle. The zinc precursor used was diethylzinc (DEZ, Sigma Aldrich). Deionized water was used as the co-reactant. The deposition recipe was 0.03/10/0.03/10 s DEZ pulse/purge/H_2O pulse/purge to ensure saturation. The growth per cycle (GPC) for ZnO was ~1.7 Å on reference Si substrate.

Preparation and Content Optimization of Reactive Suspension Electrolytes

Each reactive suspension electrolyte (RSE) was prepared by suspending the specified amount (1 to 15 wt%) of MO_x nanoparticles in RE. The nanoparticles were easily dispersed by gently shaking the mixture. Li|Cu half cells were then assembled using both the RE and the MO_x suspension electrolytes with varying concentrations (1 wt%, 5 wt%, 10 wt%, and 15 wt%). Lithium plating and stripping were performed at a current density of 1 mA cm^{-2}, and representative voltage profiles were collected (Figure S2, Supporting Information). Here, we defined a metric: consumption capacity ≡ [(current density) × (electrode area) × (time to reach 0 V vs. Li/Li^+ with the specified RSE) - (current density) × (electrode area) × (time to reach 0 V vs. Li/Li^+ with the RE)]. This metric quantified the lithium consumed in the conversion reaction and was plotted against the MO_x content (Figure S2). While the trend remained linear up to 10 wt% across all cases, the point appeared to be off the trendline with a huge variation at 15 wt%, indicating the suspension became supersaturated. Based upon this

observation, we chose 10 wt% as an optimized content for further analyses.

Cell Assembly and Electrochemical Measurements

Electrochemical tests were performed with 2032-type coin cells. For RSEs, the 10 wt% was used as a default content, otherwise indicated. For Li|Cu half cells, 20 µL of electrolytes were used. Li|Al cells with 20 µL of electrolytes were employed for linear sweep voltammetry (LSV). For the cycling test and cyclic voltammetry (CV), Li|$Li_1Ni_{0.8}Mo_{0.1}Co_{0.1}O_2$ (NMC811) cells with 30 µL of electrolyte were built. CE measurements and all cycling tests were performed using LAND instruments. The full cell cycling protocol included 0.5 C charging to 4.3 V, holding at 4.3 V until the cutoff current reached 0.05 C, followed by 1 C discharging to 3.0 V. Electrochemical Impedance Spectroscopy (EIS; from 1 MHz to 1 Hz) was performed for three replicates of each cell. For the fitting (dashed and solid lines in Figure S3), the simplified Randles circuit which consists of bulk resistance (R_s), a parallel pair of R_{SEI} and CPE 1, and the other parallel pair of R_{ct} and CPE 2. In the Nyquist plots, the x-intercept on the left (high frequency region) indicates R_s while the right end of the semicircle (low frequency region) corresponds to $R_s + R_{int}$, where R_{int} (interfacial impedance) is a sum of R_{SEI} and R_{ct}. In other words, interfacial impedance was measured as the total horizontal width of the convoluted semicircles. EIS measurements, LSV (open circuit voltage (OCV) to 5.0 V vs. Li/Li^+, scan rate = 1 mV s^{-1}), and CV (3.0 to 4.5 V vs. Li/Li^+, scan rate = 0.1 mV s^{-1}) were performed with Biologics VMP3.

Material Characterization

Scanning electron microscopy (SEM) was performed using Thermo Fisher Scientific Apreo S LoVac scanning electron microscope. For sample preparation, Li^0 of 1 mAh cm^{-2} was deposited at 1 mA cm^{-2} using Li|Cu half cells with each electrolyte. All samples were rinsed with pure diethyl carbonate (DEC) and dried in the Ar-filled glove box. X-ray photoelectron spectroscopy (XPS) was carried out using PHI Versaprobe III with a monochromatic Al Kα X-ray source. For bare MO_x nanopowder, a small scoop of particles was mounted using a double-sided tape for sample preparation. To analyze the initial SEIs, Li|Cu half cells with RE and three RSEs were discharged to 10 mV vs Li/Li^+ and held at that potential for 20 minutes. The Cu foil was then rinsed with 60 µL of DEC to remove unreacted particles and any contaminants. To avoid ambient exposure, a vacuum transfer vessel was used to migrate the sample from the glove box to the XPS transfer chamber. During the XPS scans, the pressure

inside the XPS main chamber was maintained at around 10^{-7} Pa. The obtained spectra were corrected using C 1s peak at 284.8 eV and fitted using MultiPak software. For nuclear magnetic resonance (NMR) analysis, 1D ^{7}Li NMR spectra were collected on RE and RSEs with a JEOL 500MHz NMR. For each sample, 200μL of sample was combined with 400μL DMSO-d6 (Aldrich) in a clean NMR tube sealed with a polytetrafluoroethylene cap. Cryogenic transmission electron microscopy (cryo-TEM) was conducted using FEI Titan 80-300 kV environmental transmission electron microscope with an image-forming lens aberration corrector. A lacey carbon Cu TEM grid was used as the working electrode, and 0.1 mAh cm^{-2} of Li^{0} was deposited at 1 mA cm^{-2} on top, using RE and three 1 wt% RSEs respectively. The grid was rinsed with DEC and dried, and then it was quickly plunged into liquid nitrogen without ambient exposure. While submerged in liquid nitrogen, the sample was transferred to the Gatan side-entry cryotransfer holder (Gatan model 626). The cryotransfer holder was carefully inserted into the TEM, and its temperature was maintained at approximately -178 °C. Cryo-TEM images were captured at 300 kV, and fast Fourier transform (FFT) indexing was corrected with a factor of 0.94 based on the calibration. Cryogenic scanning transmission electron microscopy (cryo-STEM) was performed with the same instrument, and cryo-STEM electron energy loss spectroscopy (EELS) mappings were acquired using the high-resolution Gatan imaging filter (GIF Quantum 966) under Dual EELS mode.